THE AMERICAN SOCIETY OF MECHANICAL ENGINEERS
345 E. 47th St., New York, N.Y. 10017

97-GT-299

Vibration Analysis of Rotating Cambered Helicoidal Turbomachine Blades

J. S. Rao

C. V. Ramakrishnan

K. Gupta

and

K. K. Rao

Indian Institute of Technology
New Delhi, India

ABSTRACT

A procedure for the vibration analysis of rotating cambered helicoidal blades using curved shell finite element based on Mindlin theory is given. The strain displacement relations of Gol den'veizer are used in the development of a thick doubly curved helicoidal shell element including initial in-plane stress effect. The method is applied to rotating cambered pretwisted blades.

INTRODUCTION

Gas turbine and compressor blades are most flexible elements and susceptible for fatigue failures. They go through several resonances before reaching the operating speed. Beam theories are inadequate to represent the dynamic behavior of wide chord blades. When they are treated as plates, the important stiffening effect of chord wise camber cannot be represented, e.g., Dokainish and Rawtani (1971) used triangular elements, Lalanne and Trompette (1974) used isoparametric elements and MacBain (1975) used quadrilateral elements. Also because of the complicated geometry of the pre-twisted blade, when plate elements are used, the coupling between membrane and bending deformation cannot take place within an element and hence more number of plate elements are needed to obtain accurate results.

A vast literature is available using classical shallow shell theories, e.g., the curved shell elements of Olson and Lindberg (1971) and Walker (1978). Ritz method is applied for rotating pre-twisted flat blades by Petricone and Sisto (1970), Gupta and Rao (1987), however, constant width, thickness and radius of curvature are assumed. Here, a procedure for the rotating cambered helicoidal blades is given using curved shell element based on Mindlin (1951) shell theory. Strain displacement relations of Golden'veizer (1961) are directly used instead of simplified relations adopted by Walker (1978), in formulating the stiffness matrix. The mass, supplementary (rotational) stiffness and centrifugal force matrices are obtained from the kinetic energy of the rotating blade. The geometric stiffness matrix is obtained by considering the strain energy due to in-plane stresses. The method is applied to determine the natural frequencies of rotating pretwisted, cambered blades. The results obtained are compared with previous literature. The effect of camber, pre-twist, speed of rotation, disc radius and setting angle on natural frequencies are studied. Results of a typical turbo machine blade are also presented.

DIFFERENTIAL GEOMETRY

The overall view of the rotating blade is shown in Fig. 1. The coordinate lines β and Y are coincident and the helicoidal coordinate line α coincides with x axis at the root of the blade and is twisted through an angle $\theta(\beta)$. The finite element mesh for the blade is considered as shown in Fig. 2 and the position vector R to any point ξ,η within the element whose local coordinate system is located at α^*,β^* is given by

$$R=\left[\alpha\cos(\theta+\phi)+h\sin(\theta+\phi)\right]I+\beta J+\left[-\alpha\sin(\theta+\phi)+h\cos(\theta+\phi)\right]K \quad (1)$$

where $\alpha=\alpha^*+\xi,\beta=\beta^*+\eta$, $h(\xi,\eta)$ is the blade camber and ϕ is the setting angle.

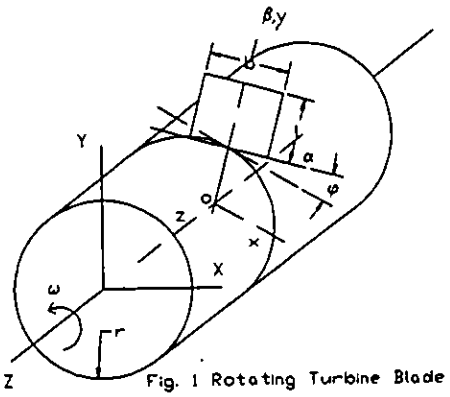

Fig. 1 Rotating Turbine Blade

Presented at the International Gas Turbine & Aeroengine Congress & Exhibition
Orlando, Florida — June 2–June 5, 1997

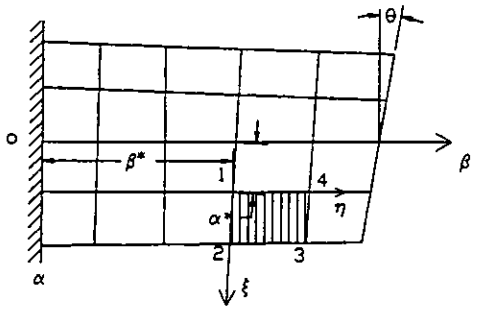

Fig. 2 Cambered Helicoidal Blade

The coefficients of first quadratic form and the radii of curvature for a shallow shell can be shown to be, see Gupta and Rao (1987)

$$A^2 = 1 \qquad B^2 = 1 + a^2\left(\theta,_\eta\right)^2$$

$$\frac{1}{R_1} = -\frac{1}{BA^2}h,_{\xi\xi}$$

$$\frac{1}{R_2} = -\frac{1}{B^3}\left[\left(\theta,_\eta\right)^2\{ah,_\xi - h\} + \theta,_{\eta\eta}\left(hh,_\xi + a\right) + h,_{\eta\eta}\right] \tag{2}$$

$$\frac{1}{R_{12}} = \frac{1}{AB^2}\left(h,_{\xi\eta} - \theta,_\eta\right)$$

The unit normal to the middle surface can be shown to be

$$\hat{n} = \frac{1}{B}\begin{bmatrix} \left\{\sin\left(\theta+\phi\right) - h,_\xi \cos\left(\theta+\phi\right)\right\}I \\ +\left\{a\theta,_\eta - h,_\eta + hh,_\xi\theta,_\eta\right\}J \\ \left[\cos\left(\theta+\phi\right) + h,_\xi \sin\left(\theta+\phi\right)\right]K \end{bmatrix} \tag{3}$$

STRAIN DISPLACEMENT RELATIONS

From Golden'veizer (1961), we can write

$$\varepsilon_{\xi\xi} = \frac{1}{A}\frac{\partial u}{\partial \xi} + \frac{v}{AB}\frac{\partial A}{\partial \eta} - \frac{w}{R_1}$$

$$\varepsilon_{\eta\eta} = \frac{1}{B}\frac{\partial v}{\partial \eta} + \frac{u}{AB}\frac{\partial B}{\partial \xi} - \frac{w}{R_2} \tag{4}$$

$$\varepsilon_{\xi\eta} = \frac{A}{B}\frac{\partial}{\partial \eta}\left(\frac{u}{A}\right) + \frac{B}{A}\frac{\partial}{\partial \xi}\left(\frac{v}{B}\right) + \frac{2w}{R_{12}}$$

$$\varepsilon_{\xi\zeta} = \Phi_\eta \quad \varepsilon_{\eta\zeta} = \Phi_\xi$$

$$\kappa_{\xi\xi} = -\frac{1}{A}\frac{\partial \Psi}{\partial \xi} - \frac{\Theta}{AB}\frac{\partial A}{\partial \eta} + \frac{\Phi}{R_{12}}$$

$$\kappa_{\eta\eta} = -\frac{1}{B}\frac{\partial \Theta}{\partial \eta} - \frac{\Psi}{AB}\frac{\partial B}{\partial \xi} - \frac{\Phi}{R_{12}} \tag{5}$$

$$\kappa_{\xi\eta} = -\frac{1}{A}\frac{\partial \Theta}{\partial \xi} + \frac{\Psi}{AB}\frac{\partial A}{\partial \eta} + \frac{\Phi}{R_1} - \frac{\varepsilon_{\eta\eta}}{R_{12}} + \frac{\varepsilon_{\xi\eta}}{2R_1}$$

$$\Theta = -\frac{1}{B}\frac{\partial w}{\partial \eta} - \frac{v}{R_2} + \frac{u}{R_{12}} + \Phi_\xi$$

$$\Psi = -\frac{1}{A}\frac{\partial w}{\partial \xi} - \frac{u}{R_1} + \frac{v}{R_{12}} + \Phi_\eta \tag{6}$$

$$\Phi = \frac{1}{2AB}\left[\frac{\partial}{\partial \eta}(Au) - \frac{\partial}{\partial \xi}(Bv)\right]$$

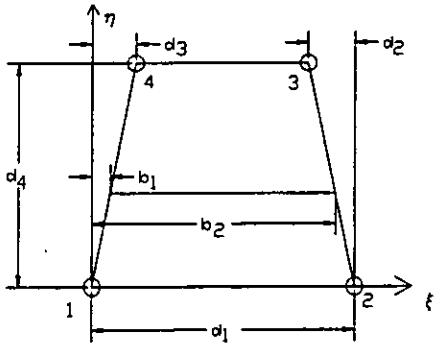

Fig. 3 Geometry of the Element

It may be noted that Walker (1978) adopted simple bending strain relations in place of equations (5) by neglecting terms containing the products of in-plane displacements with radii of curvature in equation (6).

DISPLACEMENT FUNCTIONS

The displacement functions are taken from Walker (1978) and not reproduced here. As shown in Fig. 3, each element has four nodes with sixteen degrees of freedom for each node. For a thin shell, however, there are only ten degrees of freedom for each node. The strain vector, see Walker (1978), is

$$\{\varepsilon\} = \left\{\begin{array}{cccccccc} \varepsilon_{\xi\xi} & \varepsilon_{\eta\eta} & \varepsilon_{\xi\eta} & \kappa_{\xi\xi} & \kappa_{\eta\eta} & \kappa_{\xi\eta} & \varepsilon_{\xi\zeta} & \varepsilon_{\eta\zeta} \end{array}\right\}^T = [B]\{a\} \tag{7}$$

where the 8 x 64 elements of $[B]$ can be easily derived and $\{a\}$ is the vector of coefficients of displacement functions. The thickness t in the element is approximated by a linear function.

STRAIN ENERGY

The strain energy of the thin, doubly curved helicoidal shell element in Fig. 3 is given by $U = U_I + U_{II}$, where

$$U_I = \frac{E}{2(1-\nu^2)}\int_0^{d_4}\int_{b_1}^{b_2} t\left(\xi,\eta\right) \begin{bmatrix} \left\{\begin{array}{c} \varepsilon_{\xi\xi}^2 + \varepsilon_{\eta\eta}^2 + 2\nu\varepsilon_{\xi\xi}\varepsilon_{\eta\eta} + \\ \frac{1}{2}(1-\nu)\left(\varepsilon_{\xi\eta}^2 + \gamma\varepsilon_{\xi\zeta}^2 + \gamma\varepsilon_{\eta\zeta}^2\right) \end{array}\right\} \\ +\frac{t^2(\xi,\eta)}{12}\left\{\begin{array}{c} \kappa_{\xi\xi}^2 + \kappa_{\eta\eta}^2 + 2\nu\kappa_{\xi\xi}\kappa_{\eta\eta} \\ +2(1-\nu)\kappa_{\xi\eta}^2 \end{array}\right\} \end{bmatrix} AB\,d\xi\,d\eta \tag{8}$$

is the same expression as in Walker (1978) and the strain energy due to initial stress can be written as

$$U_{II} = \frac{1}{2}\int_0^{d_4}\int_{b_1}^{b_2}\left[N_\xi^0\left(w,_\xi\right)^2 + N_\eta^0\left(w,_\eta\right)^2 + 2N_{\xi\eta}^0 w,_\xi w,_\eta\right]AB\,d\xi\,d\eta \tag{9}$$

where $b_1 = d_3\eta/d_4$, $b_2 = d_1 - d_2\eta/d_4$, γ is the shear correction factor and N^0 are initial stress resultants arising out of centrifugal force field. Eqn. (8) can be expressed as

$$U_I = \frac{1}{2}\{q\}^T[K]\{q\} \tag{10}$$

with the stiffness matrix

$$[K] = \left[[P]^{-1}\right]^T\left\{\int_0^{d_4}\int_{b_1}^{b_2}[B]^T[D][B]tAB\,d\xi\,d\eta\right\}[P]^{-1} \tag{11}$$

where $[P]$ is the transformation matrix and $\{q\}$ is the generalized displacement vector, see Walker (1978).

$$[D]=\frac{Et}{1-\nu^2}\begin{bmatrix} 1 & \nu & 0 & 0 & 0 & 0 & 0 & 0 \\ \nu & 1 & 0 & 0 & 0 & 0 & 0 & 0 \\ & & \frac{1-\nu}{2} & 0 & 0 & 0 & 0 & 0 \\ & & & \frac{t^2}{12} & \frac{\nu t^2}{12} & 0 & 0 & 0 \\ & & & & \frac{t^3}{12} & 0 & 0 & 0 \\ & & & & & \frac{(1-\nu)t^3}{6} & 0 & 0 \\ & & \text{sym} & & & & \frac{\gamma(1-\nu)}{2} & 0 \\ & & & & & & & \frac{\gamma(1-\nu)}{2} \end{bmatrix} \quad (12)$$

Equation (9) can be written as

$$U_{II}=\frac{1}{2}\int_0^{d_4}\int_{b_1}^{b_2}\begin{Bmatrix} w,_\xi & w,_\eta \end{Bmatrix}\begin{bmatrix} N^0_\xi & N^0_{\xi\eta} \\ N^0_{\xi\eta} & N^0_\eta \end{bmatrix}\begin{Bmatrix} w,_\xi \\ w,_\eta \end{Bmatrix}AB\,d\xi\,d\eta$$

Writing $\begin{Bmatrix} w,_\xi \\ w,_\eta \end{Bmatrix}=[G_1]\{a\}$, the above equation is

$$U_{II}=\frac{1}{2}\{q\}^T[K_G]\{q\} \quad (13)$$

where, the geometric stiffness matrix is

$$[K_G]=\left[[P]^{-1}\right]^T\left\{\int_0^{d_4}\int_{b_1}^{b_2}[G_1]^T[N^0][G_1]AB\,d\xi\,d\eta\right\}[P]^{-1} \quad (14)$$

KINETIC ENERGY

Making use of equations (1) and (3), the vector equation of a surface at a distance ζ from the middle surface with respect to the coordinate system fixed at the center of the disk is

$$\vec{R}(\xi,\eta,\zeta)=C_1I+C_2J+C_3K \quad (15)$$

$$C_1=\left(a-\frac{\zeta}{B}h,_\xi\right)\cos(\theta+\phi)+\left(h+\frac{\zeta}{B}\right)\sin(\theta+\phi)$$

$$C_2=\beta+r+\frac{\zeta}{B}\left(a\theta,_\eta-h,_\eta+hh,_\xi\theta,_\eta\right) \quad (16)$$

$$C_3=-\left(a-\frac{\zeta}{B}h,_\xi\right)\sin(\theta+\phi)+\left(h+\frac{\zeta}{B}\right)\cos(\theta+\phi)$$

Let u, v and $-w$ be the displacements along a,β and ζ directions respectively, then the displacements on the equidistant surface are given by

$$\begin{aligned}\overline{u}(\xi,\eta,\zeta)&=u(\xi,\eta)-\zeta\Psi\\ \overline{v}(\xi,\eta,\zeta)&=v(\xi,\eta)-\zeta\Theta\\ \overline{w}(\xi,\eta,\zeta)&=w(\xi,\eta)\end{aligned} \quad (17)$$

Taking into account of the inward displacement Δ, the displacement vector can be written as, see Golden'veizer (1961)

$$\vec{U}=\overline{u}\frac{\vec{R},_\xi}{A}+\left(\overline{v}-\Delta\right)\frac{\vec{R},_\eta}{B}-\overline{w}\hat{n} \quad (18)$$

where Δ is given by, see Rao (1991)

$$\Delta=\frac{1}{2}\int_0^\eta(\Theta^2+\Phi^2)d\eta \quad (19)$$

In Cartesian coordinates, the displacement vector is

$$\vec{U}=x_d\hat{I}+y_d\hat{J}+z_d\hat{K} \quad (20)$$

Comparing (18) and (20), we can obtain

$$\begin{aligned}x_d&=B_1u+B_2(v-\Delta)+B_3w-B_1\Psi\zeta-B_2\Theta\zeta\\ y_d&=B_4(v-\Delta)+B_5w-B_4\Theta\zeta\end{aligned}$$

$$z_d=B_{10}u+B_{20}(v-\Delta)+B_{30}w-B_{10}\Psi\zeta-B_{20}\Theta\zeta \quad (21)$$

where

$$\begin{aligned}B_1&=\frac{1}{A}\left[\cos(\theta+\phi)+h,_\xi\sin(\theta+\phi)\right]\\ B_2&=\frac{1}{B}\left[\left(-a\theta,_\eta+h,_\eta\right)\sin(\theta+\phi)+h\theta,_\eta\cos(\theta+\phi)\right]\\ B_3&=-\frac{1}{B}\left[\sin(\theta+\phi)-h,_\xi\cos(\theta+\phi)\right]\qquad B_4=\frac{1}{B}\\ B_5&=\frac{1}{B}\left(-a\theta,_\eta+h,_\eta-hh,_\xi\theta,_\eta\right)\\ B_{10}&=\frac{1}{A}\left[-\sin(\theta+\phi)+h,_\xi\cos(\theta+\phi)\right]\\ B_{20}&=\frac{1}{B}\left[\left(-a\theta,_\eta+h,_\eta\right)\cos(\theta+\phi)-h\theta,_\eta\sin(\theta+\phi)\right]\\ B_{30}&=-\frac{1}{B}\left[\cos(\theta+\phi)+h,_\xi\sin(\theta+\phi)\right]\end{aligned} \quad (22)$$

The vector equation of the deformed surface is now given by

$$\vec{R}=(C_1+x_d)I+\left(C_2+y_d\right)J+(C_3+z_d)K \quad (23)$$

$$\begin{aligned}\vec{R}=&\left[(C_1+x_d)\cos\omega t-\left(C_2+y_d\right)\sin\omega t\right]I_x\\ &+\left[(C_1+x_d)\sin\omega t+\left(C_2+y_d\right)\cos\omega t\right]I_y\\ &+(C_3+z_d)I_z\end{aligned} \quad (24)$$

The kinetic energy of the element is then given by

$$T=T_1+T_2+T_3=\frac{1}{2}\int_{-t/2}^{t/2}\int_0^{d_4}\int_{b_1}^{b_2}\rho\,\dot{\vec{R}}\cdot\dot{\vec{R}}\,AB\,d\xi\,d\eta\,d\zeta \quad (25)$$

where higher order terms of Δ are neglected and rigid body rotation terms are not included to give

$$T_1=\frac{\rho}{2}\int_{-t/2}^{t/2}\int_0^{d_4}\int_{b_1}^{b_2}\left(\dot{u}^2+\dot{v}^2+\dot{w}^2+\zeta^2\dot{\Theta}^2+\zeta^2\dot{\Psi}^2\right)AB\,d\xi\,d\eta\,d\zeta$$

$$T_2=\frac{\rho}{2}\omega^2\int_{-t/2}^{t/2}\int_0^{d_4}\int_{b_1}^{b_2}\left\{\begin{array}{c} u^2B_1^2+v^2\left(B_2^2+B_4^2\right)+w^2\left(B_3^2+B_5^2\right)+\zeta^2\Psi^2B_1^2+\\ \zeta^2\Theta^2\left(B_2^2+B_4^2\right)+2uvB_1B_2+2uwB_1B_3-2u\Psi\zeta B_1^2\\ -2u\Theta\zeta B_1B_2+2vw(B_2B_3+B_4B_5)\\ -2v\Psi\zeta B_1B_2-2v\zeta\Theta\left(B_2^2+B_4^2\right)\\ -2w\Psi\zeta B_1B_3-2w\Theta\zeta(B_2B_3+B_4B_5)\\ +2\Psi\Theta\zeta^2B_1B_2-2\Delta(B_2C_1+B_4C_2)\end{array}\right\}AB\,d\xi\,d\eta\,d\zeta$$

$$T_3=\frac{\rho}{2}\omega^2\int_{-t/2}^{t/2}\int_0^{d_4}\int_{b_1}^{b_2}\left\{\begin{array}{c} 2uB_1C_1+2v(B_2C_1+B_4C_2)+2w(B_3C_1+B_5C_2)\\ -2\Psi\zeta B_1C_1-2\Theta\zeta(B_2C_1+B_4C_2)\end{array}\right\}AB\,d\xi\,d\eta\,d\zeta \quad (26)$$

The displacement vector can be expressed as

$$\{U\} = \begin{Bmatrix} u & v & w & \Theta & \Psi \end{Bmatrix}^T = [N_1]\{a\} \quad (27)$$

so that T_1 gives the mass matrix as

$$T_1 = \tfrac{1}{2}\{\dot{q}\}^T[M]\{\dot{q}\} \quad (28)$$

$$[M] = \left[[P]^{-1}\right]^T \left\{ \rho \int_0^{d_2} \int_{b_1}^{b_2} [N_1]^T[G][N_1] AB\, d\xi\, d\eta \right\} [P]^{-1} \quad (29)$$

where

$$[G] = \begin{bmatrix} t & 0 & 0 & 0 & 0 \\ & t & 0 & 0 & 0 \\ & & t & 0 & 0 \\ & \text{sym} & & \tfrac{1}{12}t^3 & 0 \\ & & & & \tfrac{1}{12}t^3 \end{bmatrix} \quad (30)$$

Expressing $\begin{Bmatrix} \Theta & \Phi \end{Bmatrix}^T = [N_2]\{a\}$, T_2 in equation (26) gives the supplementary (rotational) stiffness matrix as

$$T_2 = \tfrac{1}{2}\{q\}^T[K_R]\{q\} \quad (31)$$

$$[K_R] = \left[[P]^{-1}\right]^T \rho\omega^2 \left\{ \int_0^{d_2} \int_{b_1}^{b_2} \begin{pmatrix} [N_1]^T[T][N_1] \\ -t(B_2B_6 + B_4B_7)\int_0^{\eta}[N_2]^T[N_2]B d\eta \end{pmatrix} AB\, d\xi\, d\eta \right\} [P]^{-1}$$

where

$$[T] = t \begin{bmatrix} B_1^2 & B_1B_2 & B_1B_3 & 0 & 0 \\ & B_2^2 + B_4^2 & B_2B_3 + B_4B_5 & 0 & 0 \\ & & B_3^2 + B_5^2 & 0 & 0 \\ & \text{sym} & & \frac{t^2}{12}\left(B_2^2 + B_4^2\right) & \frac{t^2}{12}B_1B_2 \\ & & & & \frac{t^2}{12}B_1^2 \end{bmatrix}$$

Next, the centrifugal force matrix is obtained $T_3 = \{q\}^T\{F_e\}$

$$\{F_e\} = \left[[P]^{-1}\right]^T \rho\omega^2 \int_0^{d_2} \int_{b_1}^{b_2} [N_1]^T \begin{Bmatrix} tB_1B_6 \\ t(B_2B_6 + B_4B_7) \\ t(B_3B_6 + B_5B_7) \\ \frac{t^3}{12}(B_2B_3 + B_4B_5) \\ \frac{t^3}{12}B_1B_3 \end{Bmatrix} AB\, d\xi\, d\eta \quad (34)$$

where $B_6 = a\cos\left(\theta + \phi\right) + h\sin\left(\theta + \phi\right)$ and $B_7 = \beta + r$.

Using Lagrangian equations, the elemental equations of motion can be obtained as

$$[M]\{\ddot{q}\} + ([K] + [K_G] - [K_R])\{q\} = \{F_e\} \quad (35)$$

The initial displacement vector $\{q_e\}$ due to centrifugal force is obtained from an iteration of $([K] + [K_G] - [K_R])\{q\} = \{F_e\}$. In each iteration, the geometric stiffness matrix is updated and the stress resultants are found to converge in 3 to 4 iterations. Once the geometric stiffness matrix is obtained, the elemental equations are assembled to obtain the eigen solutions. Walker's boundary conditions (1978) are used except for flat blades, where the tangential inertia term $\partial v/\partial\eta$ is also set equal to zero.

RESULTS

The results, $p\sqrt{12\varrho l^4(1-\nu^2)/Et^2}$, of Ramamurti and Kielb (1984) for $l/b = 3, b/t = 20, \theta = 30°, r/b = 2/3, \nu = 0.3, \omega/p_1 = 0.5$, are found to be in good agreement with the present values using 2x6 mesh (180 degrees of freedom) given in brackets; 4.23 (4.1923), 19.6 (19.8150), 28.01 (25.6147), 56.6 (57.0479). The discrepancy in the torsion mode 28.01, however is slightly higher, which may be attributed to the fact of fitting triangular flat plate elements to a pre-twisted shell.

The natural frequencies in Hz, of a cylindrical blade with constant thickness and radius of curvature 24" of Walker (1978) are in good agreement with the present values (4x4 mesh), 86.6 (86.76), 139.6 (140.78), 249.0 (248.45), 351.0 (353.50), 398.5 (397.37), 534.5 (525.94), 749.0 (752.55), 761.4 (761.45).

Leissa, Lee and Wang (1982) determined the natural frequencies of this blade under rotating conditions, $\omega = p_1$ and zero setting angle in Hz. They are in good agreement with the present values, 150.08 (150.68), 170.28 (180.322), 301.94 (293.137), 418.24 (415.42), 463.48 (45.867), 623.35 (572.74), 789.09 (798.566), 829.04 (802.45), except for 623.35 Hz.

For thick plates with l/b=1, b/t=8.33, and a pretwist angle 30° the non dimensional natural frequencies obtained by Sreenivasamurthy and Ramamurti (1981), using plate triangular element without shear deformation show good agreement with the present values given in brackets without shear and with shear deformation, 3.38 (3.397, 3.370), 10.19 (9.489, 9.215), 23.59 (22.80, 22.15), 30.65 (30.01, 29.13).

A cambered blade with l/b=1 and b/t=100 is chosen to study various effects. The influence of camber for a rotating plate with $\omega = p_1, r/b = 1$ and $\phi = 45°$, is given in Table 1. The bending mode stiffens with increase in camber and for a highly cambered blade, the first bending mode becomes coupled. The torsion mode also stiffens with camber, however, its stiffening is not so predominant as in the first bending, so much so, it becomes the lowest mode when camber is present. The first plate mode likewise stiffens with camber and is present for all cambered blades. The second torsion mode and other higher modes also get stiffened, which however, become coupled for highly cambered blades.

Table 1

Mode	R_1/b=1	1.5	2	2.5	∞
1	28.2-1T	22.1-1T	19.6-1T	18.3-1T	6.3-1B
2	35.9-C	27.9-1B	23.8-1B	21.0-1B	10.2-1T
3	54.2-1P	40.4-1P	35.7-1P	33.8-1P	24.6-2B
4	69.0-C	64.9-C	58.9-2T	54.7-2T	28.4-1P
5	84.4-C	69.2-C	63.6-C	60.1-C	33.9-2T
6	88.6-C	72.2-C	68.9-C	68.4-C	56.5-2P

Table 2

Mode	θ=0°	θ=10°	θ=20°	θ=30°	θ=40°
1	19.6-1T	14.5-1T	10.7-C	8.78-C	7.61-C
2	23.8-1B	26.7-C	29.1-C	27.8-C	25.9-C
3	35.7-1P	34.5-1P	39.5-1P	49.5-1P	58.5-C
4	58.9-2T	52.6-2T	54.3-C	59.4-C	61.1-C
5	63.6-C	65.0-C	72.2-C	65.4-C	64.7-C
6	68.9-C	71.1-C	73.7-C	88.4-C	104.2-C

The effect of pretwist for R_1/b=2 is given in Table 2. For a cambered plate, the effect of pretwist is substantially different from that of beams and flat plates. With a pretwist, pure bending modes disappear and get coupled. The natural frequency initially

increases with pretwist upto 20° and then decreases with further pretwist in comparison to beam type of blades where the frequency increases with pretwist and in the case of flat plates the frequency decreases with pretwist, see Rao (1991). The torsion mode is the lowest and decreases with pretwist, unlike flat blades where the torsion modes increase, see Rao (1991). The second torsion mode (fourth mode) decreases initially with small pretwist, then becomes a coupled mode and gets stiffened with further pretwist. The first plate mode (third mode) has also a similar behavior. The remaining higher modes are all coupled.

The influence of rotation for this blade is given in Fig. 4, all the modes increase with speed of rotation. In the case of flat blades, the bending modes are only effected in a significant manner, see Rao (1991), whereas for cambered plates the torsional modes are also significantly effected. For $\omega = p_1$, the influence of disc radius r/b is given in Fig. 5, all the modes increase with disk radius in the same manner as above. Fig. 6 shows the effect of setting angle, which decreases the natural frequencies. In the case of flat blades, only bending modes are somewhat effected by setting angle, see Rao (1991), whereas for cambered blades all the modes are equally effected.

The advantage of the present finite element formulation is that it can be applied to practical shell type rotating cambered blades. The case of a stationary blade data for Rolls Royce compressor blade given by Walker (1978) is chosen here to determine the natural frequencies taking into account of rotation. These results (Hz) are given in Table 3 including that of rotating blade.

Table 3

Mode	Present	Walker	Experiment	$\omega = p_1$
1	136.21	133	128	229.81
2	561.16	565	426	682.21
3	821.69	822	714	889.26
4	1,211.9	1,203	1,108	1,252.44
5	1,673.69	1,702	1,655	1,784.31

The present results for stationary blade are in good agreement with those given by Walker (1978). The experimental results quoted by Walker are also given for comparison. The present program accounts for rotational effects as well and the results obtained for $\phi = 90°, r/b_{max} = 1$ and $\omega = p_1$ are also given.

CONCLUSIONS

A curved thick shell finite element is used for the analysis of rotating cambered helicoidal turbo machine blades. Results obtained are in good agreement with the available literature. The effect of different parameters viz., camber, pretwist, rotational speed, disk radius and setting angle is presented.

NOMENCLATURE

$\{a\}$	coefficients of displacement functions
A,B	Lame's parameters
b,l,t	blade width, length and thickness
E	Young's modulus
h	blade camber
IJK	unit vectors in xyz directions
I_x, I_y, I_z	unit vectors in XYZ directions
N^0	initial stress resultants
$\hat{n}$	unit normal vector
p_1	fundamental frequency
$\{q\}$	generalized displacement vector
R_1, R_2	chord wise and span wise radii
R_{12}	radius of torsion
r	disk radius
$u,v,-w$	displacements in α,β and ζ directions
XYZ	fixed Cartesian coordinate system
xyz	rotating Cartesian coordinate system
$x_d y_d z_d$	displacements along XYZ coordinates
$\alpha\beta\zeta$	global helicoidal coordinate system
α^*, β^*	location of elemental coordinate system
γ	shear correction factor
θ	pretwist
Φ_ζ, Φ_η	transverse shear rotations
ϕ	setting angle
Δ	inward displacement
ε	membrane and shear strains
ν	Poisson's ratio
$\xi\eta\zeta$	local helicoidal coordinate system
κ	bending strains
ρ	density
ω	rotational speed
Θ, Ψ, Φ	rotations of the tangent about ξ, η, axes respectively

REFERENCES

Dokainish, M. A. and Rawtani, S., (1973) Vibration Analysis of Rotating Cantilever Plates, *Intl J Num Meth Engng*, v. 3, p. 233

Golden'veizer, A. L., (1961) *Theory of Thin Elastic Shells*, Pergammon Press

Gupta, K and Rao, J. S., (1987) Free Vibration of Rotating Small Aspect Ratio Pre-Twisted Blades, *Mech Mach Theory*, v. 22, No. 2 p. 159

Lalanne, M. and Trompette, P., (1974) Vibration Analysis of Turbine Blades, *ASME* 74-WA/DE-23

Leissa, A. W., Lee, J. K. and Wang, A. J., (1982) Rotating Blade Analysis Using Shells, *J Engng. Power, ASME*, v. 104, p. 296

MacBain, J. C.; (1975) Vibratory Behavior of Twisted Cantilever Plates, *J Aircraft*, v. 12, p. 343

Mindlin, R. D., (1951) Influence of Rotary Inertia and Shear on Flexural Motions of Isotropic, Elastic Plates, *J Appld. Mech.*, v. 18, p. 31

Olson, M. D. and Lindberg, G. M., (1971) Dynamic Analysis of Shallow Shell with a Doubly Curved Triangular Finite element, *J Sound Vib.*, v. 19, No. 3, p. 299

Petricone, R. and Sisto, F., (1970) Vibration Characteristics of Low Aspect Ratio Compressor Blades, ASME 70-GT-94

Ramamurti, V. and Kielb, R. E., (1984) Natural Frequencies of Twisted Rotating Plates, *J Sound Vib.*, v. 97, No. 3, p. 429

Rao, J. S., (1991) *Turbomachine Blade Vibration*, John Wiley

Sreenivasamurthy, S. and Ramamurti, V., (1981) A Parametric Study of Vibrations of Rotating Pre-twisted and Tapered Low Aspect Ratio Cantilever Plates, *J Sound Vib.*, v. 76, p. 311

Walker, K. P., (1978) Vibrations of Cambered Helicoidal Fan Blades, *J Sound Vib.*, Vol. 59, p 35

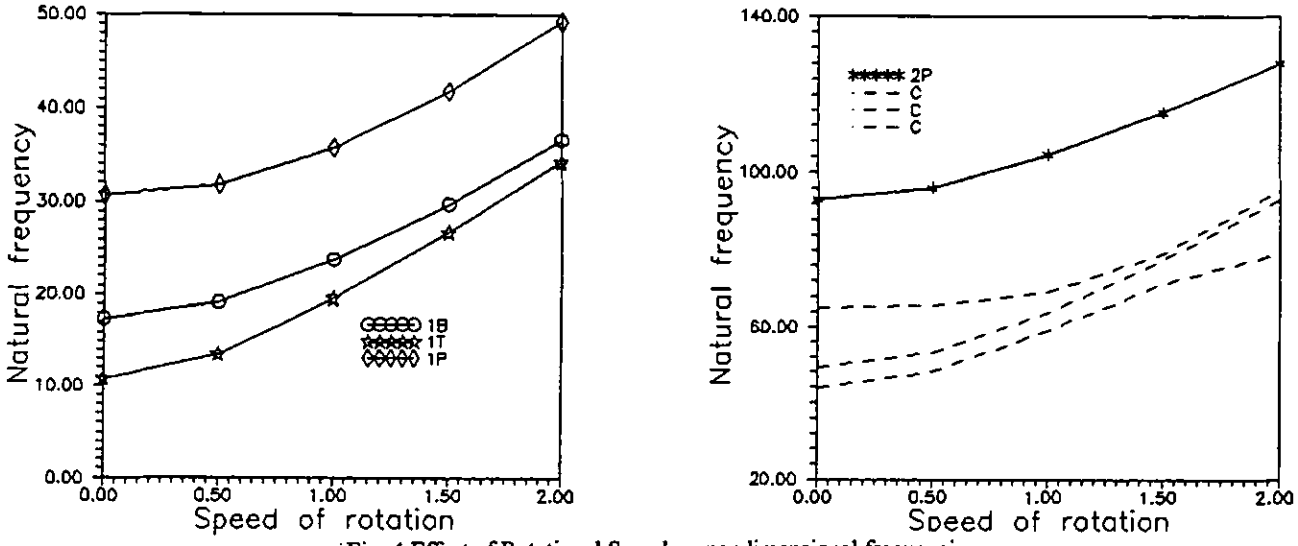

Fig. 4 Effect of Rotational Speed on nondimensional frequencies
$l/b = 1, b/t = 100, R_2/b = 2, \phi = 45°$ and $r/b = 1$.

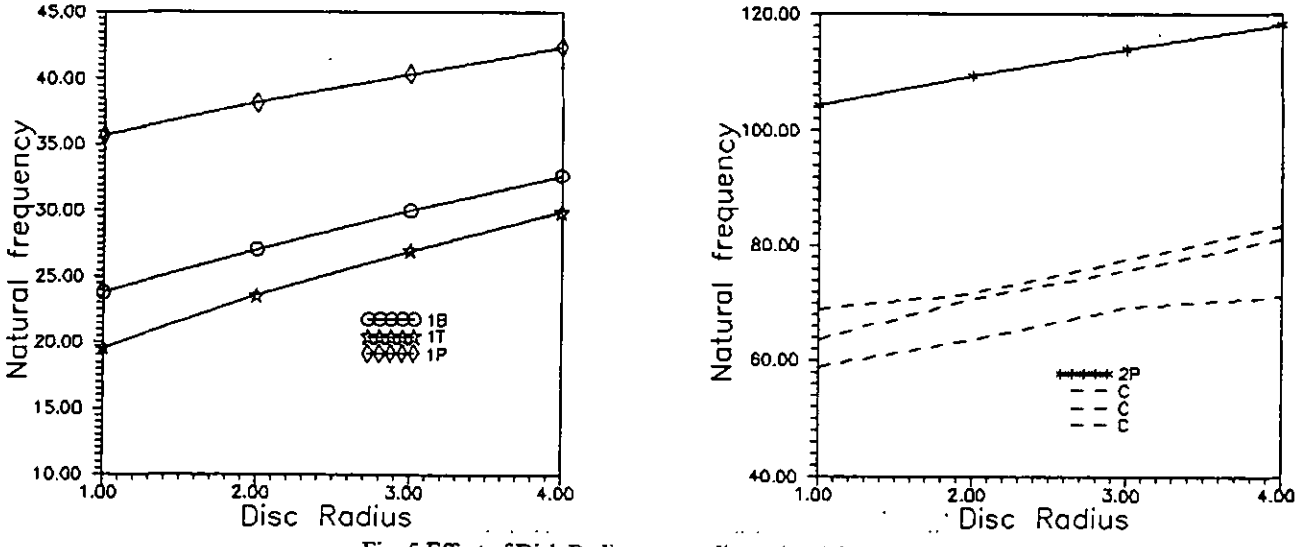

Fig. 5 Effect of Disk Radius on nondimensional frequencies
$l/b = 1, b/t = 100, R_2/b = 2, , \phi = 45°$ and $\omega = p_1$.

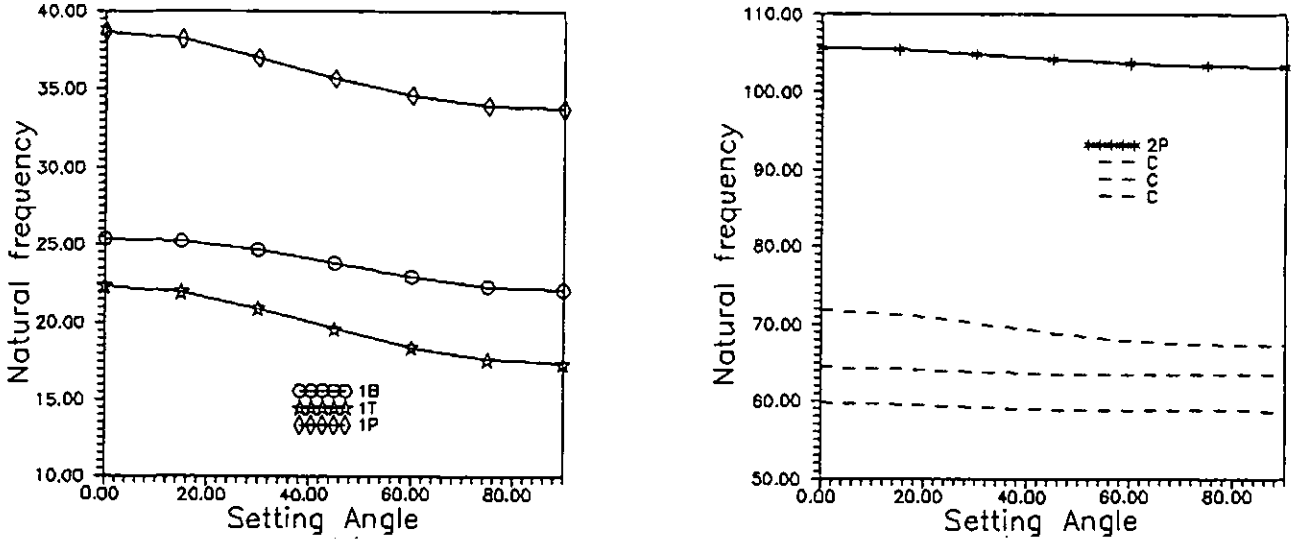

Fig. 6 Effect of Setting Angle on nondimensional frequencies
$l/b = 1, b/t = 100, R_2/b = 2, \omega = p_1$ and $r/b = 1$.